

End-to-end Temporal Action Detection with Transformer

Xiaolong Liu^{1*} Qimeng Wang¹ Yao Hu² Xu Tang² Shiwei Zhang² Song Bai¹ Xiang Bai¹
¹Huazhong University of Science and Technology ²Alibaba Group
{liuxl, qimengwang, xbai}@hust.edu.cn, songbai.site@gmail.com
{yaoohu, buhui.tx}@alibaba-inc.com

Abstract

Temporal action detection (TAD) aims to determine the semantic label and the boundaries of every action instance in an untrimmed video. Previous methods tackle this task with complex pipelines. In this paper, we propose an end-to-end temporal action detection Transformer (TadTR) with a simple set prediction pipeline. Given a small set of learnable embeddings called action queries, TadTR adaptively extracts temporal context from the video for each query and directly predicts action instances. To adapt Transformer for TAD, we propose three improvements to enhance its locality awareness. The core is a temporal deformable attention module that selectively attends to a sparse set of key snippets in a video. A segment refinement mechanism and an actionness regression head are designed to refine the boundaries and confidence of the predicted instances, respectively. TadTR requires lower computation cost than previous detectors, while preserving remarkable performance. As a self-contained detector, it achieves state-of-the-art performance on THUMOS14 (56.7% mAP) and HACS Segments (32.09% mAP). Combined with an extra action classifier, it obtains 36.75% mAP on ActivityNet-1.3. Our code is available at <https://github.com/xlliu7/TadTR>.

1. Introduction

Video understanding has become more important than ever as the rapid growth of media prompts the generation, sharing, and consumption of videos. As a fundamental task in video understanding, temporal action detection (TAD) aims to predict the semantic label and temporal interval of every action instance in an untrimmed and possibly long video. For its wide range of applications, including security surveillance, home care, video editing, and so on, temporal action detection has gained increasing attention from the community in recent years [35, 43, 28, 32, 6, 23].

As shown in Fig. 1, these pipelines involve post-

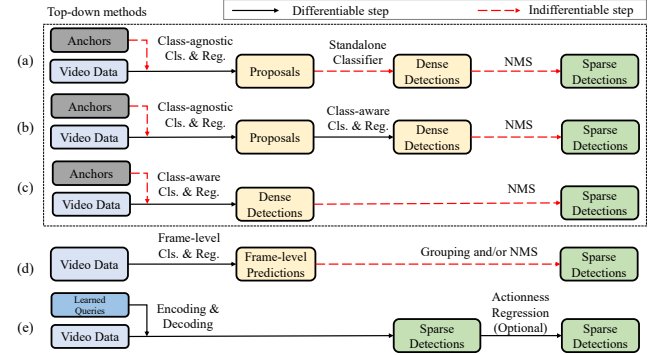


Figure 1. Comparison of different pipelines of temporal action detection. (a) Multi-stage pipeline in [35, 43], etc.; (b) Two-stage pipeline in [42, 10]; (c) Top-down one-stage pipeline in [19], (d) Bottom-up pipeline in [48] (e) The set prediction pipeline in this work.

processing operations, such as non-maximum suppression (NMS) and grouping. These operations, together with anchor setting in many top-down methods, are hand-crafted with prior knowledge about this task and not learnable, which restricts the flexibility. Besides, most proposal-based methods [49, 43, 18], requires a standalone classifier to classify action proposals. These issues block the gradient flow and prevent end-to-end learning. Thus, it is necessary to develop a simple end-to-end method that directly predicts action instances in a single differentiable network¹ without hand-crafted components.

In this paper, we propose an end-to-end Temporal Action Detection Transformer (TadTR) to simplify the pipeline of TAD. Inspired by the object detection Transformer (DETR) [8], we adapt the set prediction (SP) framework for TAD, which directly maps a small set of learnable embeddings, called action queries, to action instances in parallel with the Transformer model. TadTR has an encoder-

¹The single network means the detection network upon the video encoder. Training the video encoders along with the detection head for long videos often requires excessive computing resources. Therefore, we follow most previous methods to use offline features (e.g. I3D [9]). We explore joint learning of the encoder and the detection head in [22].

*Work done during an internship at Alibaba Group.

decoder structure. The encoder takes snippet-level video features as input and models inter-snippet relations. The decoder models the relation between queries and encoded video features and enhance the query embedding with context from the video. Upon the decoder, two feed-forward networks (FFNs) predict the class and the segment for each action query. During training, an instance matching module dynamically determines a one-to-one ground truth assignment according to the predictions. Owing to this, our detector avoids duplicate detections and NMS can be removed. It produces a very sparse set of action detections ($10 \sim 10^2$), orders of magnitude fewer than previous methods ($10^3 \sim 10^4$).

However, due to the intrinsic difference between image object detection and video action detection, a direct application of Transformer is not appropriate. To precisely detect actions, a detector needs to be *locality-aware*, which means being aware of the subtle local changes in the temporal domain. The reason is that different frames in a video of actions are highly similar due to the temporal redundancy and the slow changes in scenes/actors. However, the dense attention module in primitive Transformer that attends to all elements in a sequence, is less sensitive to such local changes by design and has difficulty in learning sparse attention to informative frames. To mitigate this issue, we draw inspiration from [56] and propose a temporal deformable attention (TDA) module as the basic building block of Transformer. It selectively attends to a sparse set of key elements around a reference location in the input sequence, where the sampling locations and attention weights are learned and dynamically adjusted in accordance with the inputs. In this way, it can adaptively extract context information while preserving locality awareness.

Besides TDA, we make two additional improvements to enhance locality awareness. First, a segment refinement mechanism is employed to refine the boundaries of predicted actions. To be concrete, we iteratively re-attend to the video according to the previous predictions and refine the boundaries with the newly extracted context. Second, we attach an actionness regression head to Transformer to predict a reliable confidence score called actionness for detection ranking. It extracts the local features with RoIAlign [15] for each predicted action and estimates its IoU with the best-matched ground truth action. This is more reliable than simply using classification scores, as the classification branch may find a shortcut from context but ignore the complete local details. Despite being seemingly small changes, they significantly improve performance.

We conduct comprehensive experiments on three datasets to validate the effectiveness of TadTR. With a surprisingly simple pipeline, TadTR achieves remarkable performance with a low computation cost. As a self-contained detector (without extra action classifiers), it achieves state-

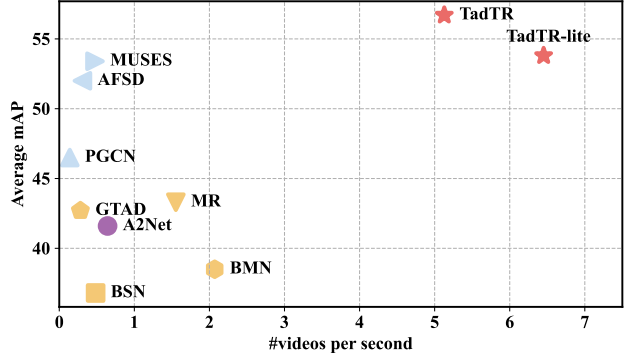


Figure 2. Comparison of recent temporal action detection methods on THUMOS14, in terms of both performance (average mAP) and speed. Our method achieves state-of-the-art performance while running significantly faster.

of-the-art performance on HACS Segments [50] and THUMOS14 [16]. When combined an extra classifier, it reaches 36.75% mAP on ActivityNet-1.3 [7], outperforming strong competitors such as G-TAD [43] and BMN [18]. In terms of run time, TadTR-lite takes only 155 ms per video on THUMOS14, which is around $14\times$ faster than the previous state-of-the-art method MUSES [23], as shown in Fig. 2. We believe that the simplicity, the flexibility, and the strong performance of the new method will benefit and ease future research on temporal action detection.

The contributions of this work are as follows:

- We introduce an end-to-end set prediction (SP) framework that simplifies the pipeline for temporal action detection (TAD). It can detect actions in a single differentiable network without hand-crafted components.
- We propose a Transformer architecture that is enhanced with locality awareness to better adapt to the TAD task. The core is a temporal deformable attention (TDA) module that selectively attends to a sparse set of key snippets in a video. We show that TDA is crucial for the success of the SP framework for TAD.
- As a self-contained detector, TadTR achieves state-of-the-art performance on HACS Segments and THUMOS14. It also demonstrate highly competitive results on ActivityNet-1.3. Besides, it requires a lower computation cost than its competitors.

2. Related Work

2.1. Temporal Action Detection Methods

Previous methods for temporal action detection can be roughly categorized into groups depending on the pipeline.

(a) **Multi-stage methods** [43, 18, 47]. They first generate candidate segments and train a binary classifier that

associates each segment with a confidence score, resulting in proposals. Those proposals with high scores are fed to a multi-class classifier to classify the actions. The candidate segments are generated by dense uniform sampling [35, 13] or grouping local frames that may contain actions [20]. Some methods [12, 24] combine multiple schemes for complementarity. (b) **Two-stage methods** [42, 10, 11, 5] simplify the multi-stage pipeline by adopting a one-stage proposal generator, which directly predicts the scores and boundaries of pre-defined multi-scale anchors associated with each temporal location. These methods need to manually set multiple anchor scales, which restricts the flexibility. (c) **Top-down one-stage methods** [19, 25] can be seen as the class-aware variant of the one-stage proposal generator. Recently, [44] augment the anchor-based one-stage detector with an anchor-free branch that makes predictions based on centers of actions. (d) A **bottom-up one-stage method** proposed in [48] first predicts the action and boundary probabilities and then groups frames with maximal structured sum as actions. We note that all the above methods require post-processing steps such as NMS or grouping, which prevent end-to-end learning.

An early work by [45] proposes an end-to-end temporal action detector based on recurrent neural networks (RNN) and reinforcement learning (RL). It learns action detection by training an agent that iteratively picking an observation location and deciding whether to emit or refine a candidate action after observation. In this work, an end-to-end Transformer-based detector significantly different from [45] is proposed. While [45] is restricted to a manner of one-by-one prediction due to the recurrent nature of RNN, our method can decode all action instances in parallel. In addition, our method is fully differentiable, whereas the RL-based method is not. All the methods discussed above are fully supervised methods. There are also some weakly supervised methods [27, 21, 30, 31, 34, 40, 46], which are beyond the scope of this paper.

2.2. Transformers for Video Understanding

Transformers [39] have achieved great success in natural language processing. The core of Transformer is the self-attention mechanism that aggregates non-local cues through a weighted sum of features at attended locations. Compared with convolutions, self-attention can capture long-range context and dynamically adjust weights according to the input. Recently, many works have revealed the great potential of Transformers in video understanding tasks. For example, VideoBert [37] and ActBert [55] utilize Transformers to learn an joint representation for video and text. TimeSformer [4] decouples spatial and temporal self-attention for video classification. Zhou *et al.* [54] capture the temporal dependency with Transformer for video captioning. Girdhar *et al.* [14] apply Transformer to model the relationship

between spatial proposals for spatio-temporal action detection.

In this paper, Transformer is used to capture temporal context information for temporal action detection. Specifically, We employ attention modules to model the relationship between video snippets, the relationship between actions and frames, and the relationship between actions. Different from many previous works where an attention module attends to all locations in the input sequence, we introduce a temporal deformable attention module that adaptively attends to a sparse set of key frames instead of all frames. Therefore, context information can be extracted without excessive computation cost. Besides adaptive context, we also employ an actionness regression head to extract aligned context in order to assign reliable confidence scores to the detections by Transformer.

2.3. Transformer-based Set Prediction Framework

TadTR introduces the transformer-based set prediction framework in DETR. Two concurrent works, AGT [29] and RTD-Net [38], also explore this framework for temporal action detection and temporal action proposal generation, respectively. However, AGT suffers from slow training convergence (1000 \times more iterations than TadTR). RTD-Net only explores proposal generation and relies on extra action classifiers to classify the proposals. Besides, it requires a three-step training scheme to optimize different parts of the network separately. In terms of performance, both of them are not competitive. Differently, TadTR can be easily optimized. In the experiments, we show that TadTR achieves much higher performance than them and also outperforms strong competitors such as MUSES [23] and AFSD [17]. Our ablation study reveals that temporal deformable attention is crucial for the success of SP-based TAD.

3. TadTR

TadTR is constructed on video features encoded with a pre-trained video classification network (*e.g.*, I3D [9]). Fig. 3 shows the overall architecture of TadTR. TadTR takes as input the video features and a set of learnable action queries. Then it outputs a set of action predictions. Each action prediction is represented as a tuple of the temporal segment, the confidence score, and the semantic label. It consists of a Transformer encoder to model the interactions between video snippets, a Transformer decoder to predict action segments, and an extra actionness regression head to estimate the confidence score of the predicted segments. During training, an instance matching module is used to determine a one-to-one ground truth assignment to the action predictions.

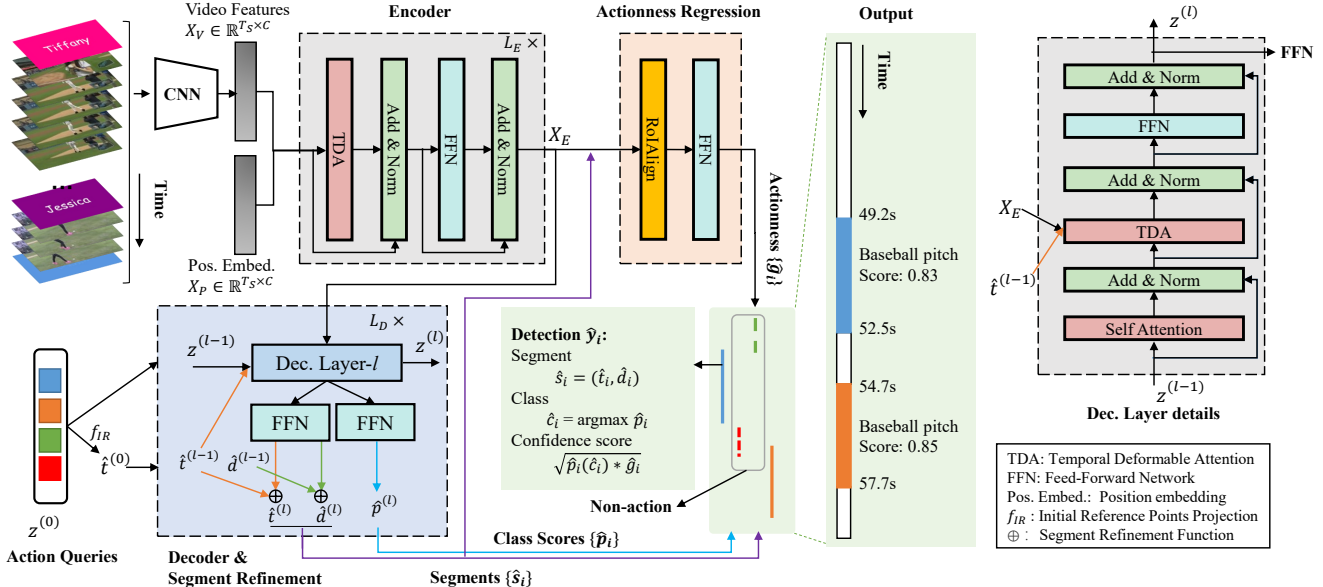


Figure 3. The architecture of TadTR. It takes the video features extracted with a CNN and a set of learnable action queries as input and decodes a set of action predictions in parallel via a Transformer. The encoder captures the long-term context in the input feature sequence. The decoder extracts relevant context from the encoder for each action query and models the relations between action queries. Upon the decoder, feed-forward networks predict the segments and the classes of the output actions. A segment refinement mechanism (the blue box) and an actionness regression head (the orange box) are utilized to refine the boundaries and the confidence scores of the predicted actions, respectively.

3.1. Architecture

Encoder. Let $\mathbf{X}_V \in \mathbb{R}^{T_S \times C}$ denotes the video feature sequence, where T_S and C are the length and dimension, respectively. Each frame in the feature sequence is a feature vector extracted from a certain snippet in the video. Here, a snippet means a sequence of a few (*e.g.*, 8) consecutive frames. We use linear projection to make $C = 256$. The encoder models the relations between different snippets and outputs a feature sequence $\mathbf{X}_E \in \mathbb{R}^{T_S \times C}$ enhanced with temporal context. As depicted in Fig. 3, it consists of L_E Transformer encoder layers of the homogeneous architecture. Each encoder layer has two sub-layers, *i.e.*, a temporal deformable attention (TDA) module, and a feed-forward network (FFN). Layer normalization [2] is used after each sub-layer and a residual connection is added between the input of each sub-layer and the output of the follow-up normalization layer. Except for TDA, all the other components are identical to the primitive Transformer [39].

TDA is an alternative to the dense attention module in [39]. The high similarities between different frames and the vagueness of action boundaries require a detector to possess locality awareness. In other words, the detector should be more sensitive to local changes in the temporal domain. The dense attention module that attends to all locations in an input feature sequence, is less sensitive to such local changes. Besides, it suffers from high computation cost and slow convergence [56]. To better fit the TAD task, we draw

inspiration from [56] and propose a temporal deformable attention (TDA) module that adaptively attends to a sparse set of temporal locations around a reference location in the input feature sequence.

Let $\mathbf{z}_q \in \mathbb{R}^C$ be the feature of query q and $t_q \in [0, 1]$ be the normalized coordinate of the corresponding reference point. Given an input feature sequence $\mathbf{X} \in \mathbb{R}^{T_S \times C}$, the output $\mathbf{h}_m \in \mathbb{R}^{T_S \times (C/M)}$ of the m -th ($m \in \{1, 2, \dots, M\}$) head of a TDA module is computed by an weighted sum of a set of key elements sampled from \mathbf{X} :

$$h_m = \sum_{k=1}^K a_{mqk} \mathbf{W}_m^V \mathbf{X}((t_q + \Delta t_{mqk})T_S), \quad (1)$$

where K is the number of sampling points, $a_{mqk} \in [0, 1]$ is the normalized attention weight, and $\Delta t_{mqk} \in [0, 1]$ is the sampling offset relative to t_q . $\mathbf{X}((t_q + \Delta t_{mqk})T_S)$ is the linear interpolated feature at $(t_q + \Delta t_{mqk})T_S$ as it is fractional. Following [56], the attention weight a_{mqk} and the sampling offset Δt_{mqk} are predicted from the query feature \mathbf{z}_q by linear projection. We normalize the attention weight with *softmax* to make $\sum_{k=1}^K a_{mqk} = 1$. $\mathbf{W}_m^V \in \mathbb{R}^{C \times (C/M)}$ is a learnable weight. The output of TDA is computed by a linear combination of the outputs of different heads:

$$\text{TDA}(\mathbf{z}_q, t_q, \mathbf{X}) = \mathbf{W}^O \text{Concat}(h_1, h_2, \dots, h_m), \quad (2)$$

where $\mathbf{W}^O \in \mathbb{R}^{C \times C}$ is a learnable weight.

When computing the τ -th frame in the output sequence, the query and the reference point are both the τ -th frame in the input sequence. Therefore, we refer to TDA in the encoder as temporal deformable self-attention (TDSA). The query feature is the summation of the input feature of that frame and the position embedding at that location. The position embedding is used to differentiate between different locations in the input sequence. In this paper, we use the sinusoidal position embedding following [39].

$$\mathbf{X}_P(\tau, \gamma) = \begin{cases} \sin \frac{\tau}{10000^{\gamma/C}} & \gamma \text{ is even} \\ \cos \frac{\tau}{10000^{(\gamma-1)/C}} & \gamma \text{ is odd} \end{cases}. \quad (3)$$

The feed-forward network consists of two fully connected (FC) layers and a ReLU activation in between. It is the same across different positions and can be viewed as a stack of two 1D convolution layers with kernel size 1. The dimensions of the two FC layers are $C_F = 2048$ and $C = 256$, respectively.

Decoder. The decoder takes as input the encoder features \mathbf{X}_E and N_q action queries with learnable embeddings $\hat{\mathbf{z}}^{(0)} = \{\hat{\mathbf{z}}_i^{(0)}\}_{i=1}^{N_q}$. It transforms these embeddings to N_q action predictions $\hat{Y} = \{\hat{y}_i\}$. As illustrated in Fig. 3, the decoder consists of L_D sequential decoder layers. Each decoder layer has three major sub-layers: a self-attention module, a temporal deformable cross-attention (TDCA) module, and a feed-forward network. Similar to each encoder layer, we add a residual connection between each sub-layer and the following layer normalization function. The output of the l -th decoder layer is denoted by $z^{(l)}$. The self-attention module models the relation between action queries and updates their embeddings. The motivation here is that multiple actions in one video are often related. For example, a cricket shot action often appears after a cricket bowling action. To make an action prediction, each query extracts relevant context information from the video via the TDCA module. Given the encoder features \mathbf{X}_E and the input embedding $\hat{\mathbf{z}}_{c,i} \in \mathbb{R}^C$, the output query embedding of TDCA is formulated as $TDA(\hat{\mathbf{z}}_{c,i}, \hat{t}_i, \mathbf{X}_E)$. Here, \hat{t}_i is the coordinate of the reference point in \mathbf{X}_E . By default, it is predicted by a projection function f_{IR} from $\hat{\mathbf{z}}_i^{(0)}$. f_{IR} is implemented with a linear layer and a follow-up *sigmoid* function for normalization. The reference point can be seen as the initial estimation of the center of the corresponding action segment. FFNs in the decoder layers have the same architecture as those in the encoder layers.

Different from TDSA in the encoder, the query embedding $\hat{\mathbf{z}}_i^{(0)}$ and the reference point are learnable and shared by all input videos. This allows the network to learn the global distribution of the action locations in the training dataset, which is more flexible than hand-crafted anchor setting or proposal sampling. An analysis is given in Sec. 4.4.

Prediction Heads. Upon the output (the updated query embeddings) of each decoder layer, we apply FFNs to predict the classification probabilities $\hat{\mathbf{p}}_i$ and the temporal segment $\hat{s}_i = (\hat{t}_i, \hat{d}_i)$ of the action instance \hat{y}_i corresponding to each query. Both \hat{t}_i and \hat{d}_i are normalized. To make the boundaries of the instances more accurate, a segment refinement mechanism is proposed. Besides, an additional actionness regression head is employed to refine the confidence score. They are detailed below.

Segment Refinement. Transformer is able to capture long-range context information. However, the predicted action boundaries might be unsatisfactory for lack of locality. Inspired by [56], we introduce a refinement mechanism to enhance locality awareness and improve localization performance. It involves two strategies. The first is the incremental refinement of segments. Instead of predicting the segments independently at each decoder layer, we adjust the segments according to previously predicted segments layer by layer. Formally, given each action segment $\hat{s}_i^{(l-1)} = (\hat{t}_i^{(l-1)}, \hat{d}_i^{(l-1)})$ predicted at the $(l-1)$ -th decoder layer, the l -th decoder layer predicts the location offsets $(\Delta\hat{t}_i^{(l)}, \Delta\hat{d}_i^{(l)})$ relative to $\hat{s}_i^{(l-1)}$. The corresponding refined segment $\hat{s}_i^{(l)} = (\hat{t}_i^{(l)}, \hat{d}_i^{(l)})$ is then computed by:

$$\hat{t}_i^{(l)} = \sigma(\Delta\hat{t}_i^{(l)} + \sigma^{-1}(\hat{t}_i^{(l-1)})), l \in \{1, 2, \dots, L_D\} \quad (4)$$

$$\hat{d}_i^{(l)} = \sigma(\Delta\hat{d}_i^{(l)} + \sigma^{-1}(\hat{d}_i^{(l-1)})), l \in \{2, 3, \dots, L_D\}, \quad (5)$$

where $\sigma(\cdot)$ and $\sigma^{-1}(\cdot)$ are the sigmoid and the inverse sigmoid function, respectively. Specially, $\hat{t}_i^{(0)}$ is the initial reference point \hat{t}_i predicted by f_{IR} . The initial value of $\hat{d}_i^{(l)}$ is $\hat{d}_i^{(1)}$ predicted at the first decoder layer. The second is iterative reference point adjustment. We update the reference points of TDCA in each decoder layer instead of always using $\hat{t}_i^{(0)}$. Specifically, $\hat{t}_i^{(l-1)}$, the refined segment center at the $(l-1)$ -th decoder layer, is used as the reference point of TDCA at the l -th decoder layer. In this way, TDCA can be adaptive to the input video and better aligned with the local features of the action instances.

Actionness Regression. One challenge of temporal action detection is to generate reliable confidence scores for ranking. Typically, classification scores are used. However, the classification task focuses more on discriminative features and is less sensitive to the localization quality of an action. As a result, the classification score of the detections may be unreliable for ranking. An example is shown in Fig. 4.

To mitigate this issue, we employ an actionness regression head that extracts context aligned with the interval of a predicted segment and predicts an actionness score upon it. Given the encoder feature sequence \mathbf{X}_E and a predicted segment \hat{s}_i by the decoder, we first apply temporal ROIAlign [15] upon \mathbf{X}_E to obtain the aligned features $\mathbf{X}_{s_i} \in \mathbb{R}^{T_R \times C}$ within the interval defined by s_i from



Figure 4. The Transformer may generate unreliable confidence scores. Here, a prediction with a lower overlap with the curling action has a higher score than a more accurate prediction (0.50 vs. 0.39).

X_E . Here, T_R is the number of bins for RoIAlign. To include a certain amount of context information around the boundaries, we slightly expand the segment by a factor of ϵ when applying RoIAlign. The expanded segment can be expressed as $(\hat{t}_i, \epsilon \hat{d}_i)$. Then, a feed-forward network is used to predict the actionness score \hat{g}_i from the aligned feature. \hat{g}_i is supervised by the maximal IoU g_i (intersection over union) between s_i and all ground truth actions. In this way, the detector is enforced to be more sensitive to local features in order to differentiate between different segments.

3.2. Training and Inference

Instance Matching. The instance matching module determines the targets assigned to each detection during training. Inspired by DETR [8] in object detection, we frame it as a set-to-set bipartite matching problem to ensure a one-to-one ground truth assignment.

Let $Y = \{y_j\}_{j=1}^{N_q}$ be a set of ground truth actions padded with \emptyset (no action) and π be the permutation that assigns each target y_j to the corresponding detection $\hat{y}_{\pi(j)}$. Bipartite matching aims to find a permutation that minimizes the overall matching cost:

$$\hat{\pi} = \arg \min \sum_{j=1}^{N_q} \mathcal{C}(y_j, \hat{y}_{\pi(j)}). \quad (6)$$

The matching cost considers the classification probabilities and the distance between ground truth and predicated segments. Specifically, $\mathcal{C}(y_j, \hat{y}_{\pi(j)})$ is defined as

$$\mathbb{1}_{c_j \neq \emptyset} [\mathcal{L}_{cls}(\hat{p}_{\pi(j)}, c_j) + \mathcal{L}_{seg}(s_j, \hat{s}_{\pi(j)})], \quad (7)$$

where c_j and s_j are the class label and the temporal segment of y_j . $\mathcal{L}_{cls}(\hat{p}_{\pi(j)}, c_j)$ is the classification term. We use cross-entropy loss by default. $\mathcal{L}_{seg}(s_j, \hat{s}_{\pi(j)})$ is the distance between the predicted location and the ground truth location, defined as

$$\lambda_{iou} \mathcal{L}_{iou}(s_j, \hat{s}_{\pi(j)}) + \lambda_{coord} \mathcal{L}_{L1}(s_j, \hat{s}_{\pi(j)}), \quad (8)$$

where \mathcal{L}_{L1} is the L_1 distance and \mathcal{L}_{iou} is the IoU loss. IoU loss is defined as the opposite number of the IoU. λ_{iou} and λ_{coord} are hyper-parameters. The matching problem is solved with the Hungarian algorithm.

Through the set-based instance matching, each ground truth will be assigned to only one prediction, thus avoiding duplicate predictions. This brings two merits. First, TadTR does not rely on the non-differentiable non-maximal suppression (NMS) for post-processing and enjoys end-to-end training. Second, we can make sparse predictions with limited queries (e.g. 10) instead of dense predictions in many previous works (e.g. tens of thousands for BMN [18] and G-TAD [43]), which saves the computation cost.

In a way, the instance matching module performs a learnable NMS. The matching cost takes the classification scores of the detections into account. In this way, those detections with lower scores are more likely to be assigned with a non-action target. As a result, their classification scores will be suppressed in the training process.

Loss Functions. Once the ground truth assignment is determined, we optimize the network by minimizing the following multi-part loss functions:

$$\begin{aligned} \mathcal{L} = \sum_{j=1}^{N_q} & [\mathcal{L}_{cls}(\hat{p}_{\hat{\pi}(j)}, c_j) + \mathbb{1}_{c_j \neq \emptyset} \mathcal{L}_{seg}(s_j, \hat{s}_{\hat{\pi}(j)}) \\ & + \lambda_{act} \mathcal{L}_{L1}(\hat{g}_{\hat{\pi}(j)}, g_{\hat{\pi}(j)})], \end{aligned} \quad (9)$$

where the first two items optimize the detections from the decoder and the last one optimizes the outputs of actionness regression. $\hat{\pi}$ is the solution of Equation 6. λ_{act} is a hyper-parameter.

Inference. During inference, we ignore the action predictions from all but the last decoder layer. The confidence score for a detection \hat{y}_i is computed by $\sqrt{\hat{p}_i(\hat{c}_i) \cdot \hat{g}_i}$, where \hat{c}_i is the predicted action label.

4. Experiments

4.1. Experimental Setup

Datasets and Evaluation Metrics. We conduct experiments on THUMOS14 [16], HACS Segments [50], and ActivityNet-1.3 [7]. THUMOS14 is built on videos from 20 sports action classes. It contains 200 and 213 untrimmed videos for training and testing. There are 3007 and 3358 action instances on the two sets. ActivityNet-1.3 and HACS Segments share the same 200 classes of daily activities. Both datasets are split into three sets: training, validation, and testing. The numbers of videos in these sets are 10024, 4926, and 5044 respectively on ActivityNet-1.3, and 37613, 5981, and 5987 on HACS Segments. On both datasets, the annotations on the testing set are reserved by the organizers. Therefore, we evaluate on the validation set.

Following conventions, the mean average precision (mAP) at different IoU thresholds is used for performance evaluation. On THUMOS14, the IoU thresholds for computing mAPs are $[0.3 : 0.7 : 0.1]$. On the other two datasets,

we report mAPs at the thresholds $\{0.5, 0.75, 0.95\}$ and the average mAP at the thresholds $[0.5 : 0.95 : 0.05]$.

Video Feature Extraction. Most TAD methods are based on offline extracted video features. For easier comparison with them, we also use video features as the input of our method. For experiments on HACS Segments, we directly use the official I3D features², which are extracted with I3D trained on Kinetics at 2FPS (frame per second). On THUMOS14, the two-stream I3D [9] networks pre-trained on Kinetics [9] are taken as the video encoder, and the features are extracted every 8 frames. On ActivityNet-1.3, we use the two-stream TSN [41] features extracted at 5FPS by default. We also conduct experiments with the I3D[9] features³ and TSP [1] features⁴.

Implementation Details. The dimension of the feed-forward network is 2048. C is set to 256. L_E and L_D are set to 2 and 4, respectively. The loss weights λ_{iou} , λ_{coord} and λ_{act} are set to 2, 5 and 5 respectively. The numbers of attention heads M and sampling points K are set to 8 and 4, respectively. The parameters of the linear layers that predict attention weights are initialized to zero. We initialize the linear layers that predict sampling offsets to make $\{\Delta p_{mjk}\}_{m=1}^8 = (k, 0, -k, 0, k, 0, -k, 0)$ at initialization. The expanding factor ϵ and the number of bins T_R for RoIAlign in the actionness regression head are 1.5 and 16 respectively. The number of queries are 40, 10, 30 for THUMOS14, ActivityNet-1.3, and HACS Segments, respectively.

TadTR is trained using AdamW [26] optimizer. The initial learning rate is 2×10^{-4} and scaled by a factor of 0.1 after training for a certain number of epochs. The learning rates of the linear projection layers for predicting attention weights and sampling offsets are multiplied by 0.1. The batch size is set to 16. We train the models for 16, 12, and 20 epochs and decrease the learning rate after 14, 9, and 18 epochs on THUMOS14, ActivityNet-1.3, and HACS Segments respectively. It takes around 10 minutes, 36 minutes, and 150 minutes to finish training on THUMOS14, ActivityNet-1.3, and HACS Segments, respectively. For the classification cost \mathcal{L}_{cls} in Equation 7, we also try the negative probability $-\hat{p}_{\pi(j)}(c_j)$ following DETR (\mathcal{L}_{cls} in Equation 9 still uses focal loss). In this setting, the models are trained for 30 epochs and the learning rate is decreased after 25 epochs.

Following previous works [18, 43], we resize the video features to a fixed length of 100 via linear interpolation on ActivityNet-1.3 and HACS Segments. Since the videos are long on THUMOS14, we use a sliding window strategy for training and inference. In some cases, an action instance

²http://hacs.csail.mit.edu/hacs_segments_features.zip

³<https://github.com/Finspire13/CMCS-Temporal-Action-Localization>

⁴<https://github.com/HumanAlwassel/TSP>

only partially falls into a window, which causes trouble for training. Inspired by G-TAD [43] and AFSD[19], we use an integrity-based instance filtering strategy to deal with such cases. In each window, we only keep those action instances whose integrity exceeds 0.75 for training. Here, the integrity of an instance s_g in a window s_w is defined as $|s_g \cap s_w|/|s_g|$, where $|\cdot|$ means the length. The window length is 128. The stride is 64 for training. During inference, the stride is increased to 96 and the duplicate detections in the overlapped region are merged with NMS. This strategy is called cross-window fusion (CWF). We also report the performance of TadTR tested on non-overlapping windows (with a stride of 128). In this case, we simply take the union of detections from all windows of a video.

The experiments are conducted on a workstation with a single Tesla P100 GPU card, and Intel(R) Xeon(R) CPU E5-2682 v4 @ 2.50GHz.

4.2. Main Results

THUMOS14. Table 1 demonstrates the temporal action detection performance and run time comparison on the testing set of THUMOS14. We measure the run time of these methods with publicly available implementations under the same environment (a single P100 GPU). We run methods on the full testing set with batch size set to 1 and report the average time and FLOPs per video. The computation cost of the feature extractor these methods is not included. The average length of videos on THUMOS14 is 217 seconds. BMN [18] and G-TAD [43] use two-stream TSN [41] features originally. For fair comparison, we also report their performance with I3D features. For TadTR, we report the performance with different inference settings. TadTR performs dense testing on overlapped windows. TadTR-lite is the variant that performs testing on non-overlapped windows. We observe that:

1) TadTR achieves the best performance among all the compared methods in terms of mAP at all IoU thresholds. Even the lightweight variant TadTR-lite maintains the superiority in average mAP. TadTR outperforms the second-best method MUSES [23] by 3.3% in terms of average mAP, which demonstrates the advantage of our method. Compared with the competitive single-network method A2Net [44], TadTR achieves 15.1% higher average mAP.

2) Compared with the concurrent Transformer-based methods AGT [29] and RTD-Net [38], TadTR achieves better performance. It surpasses AGT by 9.7% in terms of mAP@0.5. It also outperforms RTD-Net by 7.7% (56.7% vs. 49.0%) in terms of average mAP. Besides the advantage in accuracy, TadTR is easier to train. Differently, AGT requires 1000 \times more training iterations (3000k vs. 3k for TadTR) due to slow convergence of dense attention. RTD-Net requires a three-step training scheme to optimize

Table 1. Comparison with state-of-the-art methods on THUMOS14. Run time is the average inference time per video, including post-processing operations, such as NMS. For methods that only implement proposal generation, the run time of the external classifier is not included (marked with $>$). E2E: end-to-end. TS: two-stream. SN: single-network. * Results copied from [44]. ** Our implementation.

Method	Feature	SN	E2E	0.3	0.4	0.5	0.6	0.7	Avg.	Time/ms	FLOPs/G
BSN [20]	TS	-	-	53.5	45.0	36.9	28.4	20.0	36.8	>2065	>3.4
BMN [18]	TS	-	-	56.0	47.4	38.8	29.7	20.5	38.5	>483	>171.0
BC-GNN [3]	TS	-	-	57.1	49.1	40.4	31.2	23.1	40.2	-	-
G-TAD [43]	TS	-	-	54.5	47.6	40.2	30.8	23.4	39.3	>4440	>639.8
TAL-Net [10]	I3D	✓	-	53.2	48.5	42.8	33.8	20.8	39.8	-	-
BMN* [18]	I3D	-	-	56.4	47.9	39.2	30.2	21.2	39.0	-	-
G-TAD** [43]	I3D	-	-	58.7	52.7	44.9	33.6	23.8	42.7	>3552	>368.9
MR [51]	I3D	-	-	53.9	50.7	45.4	38.0	28.5	43.3	>644	>36.8
A2Net [44]	I3D	✓	-	58.6	54.1	45.5	32.5	17.2	41.6	1554	30.4
P-GCN [49]	I3D	-	-	63.6	57.8	49.1	-	-	-	7298	4.4
P-GCN** [49]	I3D	-	-	64.9	59.0	49.4	36.7	22.6	46.5	7298	4.4
PCG-TAL [36]	I3D	-	-	64.2	57.3	48.3	-	-	-	-	-
AGT [29]	I3D	✓	✓	65.0	58.1	50.2	-	-	-	-	-
RTD-Net [38]	I3D	-	-	68.3	62.3	51.9	38.8	23.7	49.0	>211	>32.1
AFSD [17]	I3D	-	-	67.3	62.4	55.5	43.7	31.1	52.0	3245	84.1
MUSES [23]	I3D	-	-	68.9	64.0	56.9	46.3	31.0	53.4	2101	34.1
TadTR (Ours)	I3D	✓	✓	74.8	69.1	60.1	46.6	32.8	56.7	195	0.94
TadTR-lite (Ours)	I3D	✓	✓	71.3	65.9	57.0	44.6	30.4	53.8	155	0.75

different parts of the network.

3) Our results are achieved at a low computation cost. TadTR is around $11\times$ faster than the second-best method MUSES, and $8\times$ faster than the competitive single-network detector A2Net. TadTR-lite is even faster than TadTR. It also requires much fewer FLOPs. The efficiency of our method is owing to the simple framework and the sparsity of predictions.

The above results indicate that our method is both accurate and efficient. We also note that many other methods are composed of multiple independently trained networks. Those proposal generation methods (BSN, MGG, BMN, G-TAD, MR, BC-GNN, and RTD-Net) are not self-contained, as they rely on an extra classifier (such as P-GCN) to accomplish the TAD task. Differently, TadTR can achieve action detection with only a *single* unified network.

HACS Segments. This is a recently introduced dataset, therefore the results of many early methods on this dataset are not available. We report the performance of TadTR, SSN [52], and the state-of-the-art method G-TAD [43] in Table 2. With the default setting, our method achieves an average mAP of 32.09%, which clearly outperforms SSN (+13.12% mAP) and G-TAD (+4.61% mAP). Besides, our method requires $455\times$ less computation cost than G-TAD. As for run time, the network inference and post-processing step of G-TAD take 33 ms and 908 ms per video, respectively. The total run time is 941 ms, $49.5\times$ that of TadTR (19 ms). The results again illustrate the superiority of TadTR.

Table 2. Comparison of different methods on HACS Segments. The results of SSN are from [50]. The magnitude is Mega (10^6) for FLOPs.

Method	0.5	0.75	0.95	Avg.	FLOPs
SSN [53]	28.82	18.80	5.32	18.97	-
G-TAD [43]	41.08	27.59	8.34	27.48	45725.9
TadTR (Ours)	47.14	32.11	10.94	32.09	100.5

ActivityNet-1.3. Table 3 compares the performance of different methods on the validation set of ActivityNet-1.3. Some methods, such as G-TAD, only implement action proposal generation and cannot produce action detections without external action classifiers. We divide the methods into two groups according to whether extra action classifiers are used. We refer to methods that do not use extra action classifiers as self-contained methods. As a self-contained detector, TadTR achieves an average mAP of 29.90%, which is much stronger than the other methods with more complex pipelines such as PCG-TAL [36] and P-GCN [49]. It surpasses the second-best method PCG-TAL by 2.56% higher in terms of mAP. Compared with the second-best single-network detector TAL-Net, we improve the performance by 9.68%. We also evaluate TadTR with TSP [1] features. With the new features, the average mAP is boosted to from 29.90% to 33.85%.

For comparison with previous methods [43, 18, 44] that are combined with extra classifiers [53], we also try such a combination. To be concrete, we pass the detections by

Table 3. Comparison of different methods on ActivityNet-1.3. Methods in the second group are combined with extra action classifiers [53]. The computation costs (in FLOPs) of the action classifiers are not included. TS: two-stream. SN: single-network.

Method	Feature	SN	E2E	0.5	0.75	0.95	Avg.	FLOPs/G
<i>Self-contained methods</i>								
CDC [33]	C3D	-	-	43.83	25.88	0.21	22.77	-
R-C3D [42]	C3D	✓	-	26.8	-	-	-	-
SSN [52]	TS	-	-	39.12	23.48	5.49	23.98	-
TAL-Net [10]	I3D	✓	-	38.23	18.30	1.30	20.22	-
P-GCN [49]	I3D	-	-	42.90	28.14	2.47	26.99	5.0
PCG-TAL [36]	I3D	-	-	42.14	28.34	6.12	27.34	-
TadTR (Ours)	TS	✓	✓	43.67	30.58	8.32	29.90	0.038
TadTR (Ours)	TSP	✓	✓	50.06	34.51	9.06	33.85	0.038
<i>Combined with extra classifiers</i>								
BMN [18]	TS	-	-	50.07	34.78	8.29	33.85	45.6
P-GCN [49]	I3D	-	-	48.26	33.16	3.27	31.11	5.0
G-TAD [43]	TS	-	-	50.36	34.60	9.02	34.09	45.7
MR [51]	I3D	-	-	43.47	33.91	9.21	30.12	-
A2Net [44]	I3D	-	-	43.55	28.69	3.70	27.75	1.2
PCG-TAL [36]	I3D	-	-	50.24	35.21	7.84	34.01	-
RTD-Net [38]	I3D	-	-	47.21	30.68	8.61	30.83	3.1
AFSD [17]	I3D	-	-	<u>52.38</u>	<u>35.27</u>	6.47	34.39	3.3
TadTR (Ours)	TS	-	-	51.29	34.99	<u>9.49</u>	<u>34.64</u>	0.038
TadTR (Ours)	I3D	-	-	52.83	37.05	10.83	36.11	0.038
BMN [18]	TSP	-	-	51.23	36.78	9.50	35.67	45.6
G-TAD [43]	TSP	-	-	51.26	37.12	9.29	35.81	45.7
TadTR (Ours)	TSP	-	-	53.62	37.52	10.56	36.75	0.038

TadTR to the classifiers and fuse the classification scores of TadTR and the classifiers by multiplication. When fused with [52], TadTR enjoys a significant performance boost, achieving an average mAP of 34.64%. It is better than the other compared methods in terms of average mAP, although some of them use the stronger I3D features. When TadTR uses the I3D features, the average mAP is further boosted to 36.11%, outperforming the second-best method AFSD by 1.72%. Compared with RTD-Net, the average mAP is improved by 5.23%. Besides, the computation cost of TadTR is lower, as indicated by the smaller FLOPs. In this setting, we also explore TSP [1] features. The performance of TadTR reaches 36.75% mAP, outperforming G-TAD by 0.94% and BMN by 1.08% when they use the same features. It demonstrates the superiority of TadTR again.

4.3. Ablation Study

In this subsection, we evaluate the effects of the key components of TadTR and the hyper-parameters on HACS Segments. Unless specially noted, these experiments use the negative probability for the classification cost instance matching.

The importance of context information. The key of

Transformer is the self-attention mechanism that incorporates the context in a video sequence. In TadTR, we leverage two kinds of context, inter-snippet context from all snippets and inter-action context from all action queries. They are captured by Transformer encoder and the self-attention module in Transformer decoder respectively. We report the performance of the variants that remove them respectively in Table 4. It is observed that removing the encoder leads to a significant performance drop of 3.99% average mAP. It indicates that the Transformer encoder is crucial for our model, as the decoder requires long-range and adaptive context to reason the relations between the actions and the video. Removing instance-level context, the average mAP drops by 1.13%. We conclude that the context information between action instances is also helpful.

Transformer encoder v.s. CNN encoder. We try replacing the Transformer encoder with a 1D CNN encoder, which is common for temporal modeling in previous TAD methods. The 1D CNN encoder is composed of two 1D convolutional layers with 256 filters of kernel size 3 and ReLU activation. As can be observed in Table 5, using 1D CNN encoder leads to 2.88% average mAP drop when NMS is not applied (the default option), and 1.41% average mAP drop when NMS is

Table 4. Ablation study on HACS Segments. Diff: performance difference with the standard model.

Variants	0.5	0.75	0.95	Avg.	Diff	FLOPs/M
TadTR	45.16	30.70	11.78	30.83	-	100.5
TadTR w/o encoder	39.65	26.99	9.08	26.94	-3.99	95.3
TadTR w/o instance-level context	43.11	29.97	10.43	29.70	-1.13	66.8
TadTR with dense attention	22.76	12.52	4.19	13.58	-17.25	564.5
TadTR w/o actionness regression	42.10	28.44	10.23	28.51	-2.32	99.4
TadTR w/o segment refinement	39.89	28.03	9.54	27.65	-3.18	99.8

Table 5. Comparison of the variants of TadTR with Transformer encoder and 1D CNN encoder on HACS Segments.

Encoder	Average mAP		FLOPs/M
	w/o NMS	w/ NMS	
Transformer	30.83	30.53	100.5
1D CNN	27.95(-2.88)	29.12(-1.41)	134.8

applied. Interestingly, the performance of this variant with NMS is improved by 1.17% over that without NMS. It indicates that there are many duplicate detections. One possible reason is that CNN features are locally correlated. Therefore, it is hard to differentiate between close detections as they have similar features.

To further dissect the performance gap between TadTR with 1D CNN encoder (equipped with NMS) and TadTR, we divide the ground truth instances into 3 groups according to the normalized duration: short ($0 \sim 0.1$), medium ($0.1 \sim 0.2$) and long ($0.2 \sim 1$) and report the average mAP for each group in Fig. 5. Here we use the normalized duration because we resize the video features into a fixed length. For reference, the average duration per video is 148 seconds. As can be observed, TadTR with Transformer encoder achieves better performance for medium-length and long actions. 1D CNN encoder is slightly better for short actions. The result is reasonable, as 1D CNN is good at modeling short-term dependency but poor at modeling long-term dependency.

We also explore deeper CNNs and larger convolution kernels, but no improvement is observed. In terms of computation cost, this variant has much higher FLOPs than TadTR with Transformer encoder. The results show that 1D CNN is inferior to Transformer encoder.

Dense attention v.s. temporal deformable attention. We try replacing all temporal deformable attention modules in TadTR with vanilla dense attention modules. This variant is called “TadTR with dense attention”. As depicted in Table 4, the performance of this variant is far behind TadTR (13.58% v.s. 30.83% average mAP). It indicates that temporal deformable attention is crucial for the success of TadTR. Besides, it has $5.7 \times$ higher computation cost than that of TadTR. The main reason is that the dense attention lacks induced bias. A dense attention module is initialized to nearly take an average of all locations in the input sequence ap-

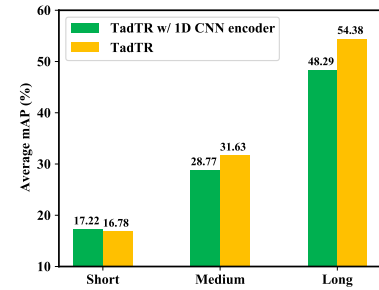


Figure 5. Comparison of the performance of TadTR with 1D CNN encoder and TadTR (with Transformer encoder) for actions with different durations on HACS Segments.

proximately. It is hard to learn to focus on specific locations. Therefore, temporal deformable attention is a better choice.

Effects of actionness regression and segment refinement. We study the effects of iterative segment refinement and actionness regression by removing them from TadTR individually, resulting in 2 different model variants. Their results on HACS Segments are presented in Table 4. Comparing TadTR w/o actionness regression and TadTR, we observe that actionness regression leads to improvements of all metrics. Specifically, the improvements are 3.06%, 2.26%, 1.55%, and 2.32% in terms of mAP at IoU 0.5, 0.75, 0.95 and the average mAP. Several qualitative examples are presented in Fig. 6 to show how actionness regression helps. It is able to produce more reliable confidence scores for the action predictions by Transformer, owing to explicit feature alignment. Comparing TadTR w/o segment refinement and TadTR, we find this component helpful for improving the localization accuracy. It improves the mAP at the strict threshold of 0.95 by a large margin of 2.24%. The mAPs at other thresholds are also consistently improved.

Besides the detection performance, another important aspect is the computation cost of the detector. In terms of FLOPs, adding or removing the two components has little impact, which is shown in Table 4. In terms of run time, we keep the same environment used in Fig. 2 and Table 1 for run time measurement. The average time cost per video is 130 ms without the two components. Adding the actionness regression module will increase the average time cost

Table 6. Effect of numbers of encoder layers and decoder layers. The detection performance is evaluated on HACS Segments.

L_E	L_D	0.5	0.75	0.95	Avg.	FLOPs/M
2	4	45.16	30.70	11.78	30.83	100.5
4	4	44.63	30.39	10.76	30.39	105.6
6	4	40.55	27.55	9.88	27.63	110.8
2	2	42.10	29.05	9.57	28.84	79.6
2	4	45.16	30.70	11.78	30.83	100.5
2	6	45.20	30.82	10.67	30.74	121.3

Table 7. Impact of the number of sampling points K on the performance and computation cost on HACS Segments. The models are trained for half of the full training cycle (15 epochs).

# points	0.5	0.75	0.95	Avg.	FLOPs/M
1	39.22	27.07	9.80	27.03	99.1
2	40.22	27.62	10.15	27.61	99.6
4	41.20	28.52	10.63	28.49	100.5
8	39.77	27.15	9.86	27.20	102.4

Table 8. Effect of the number of attention heads M on the performance and computation cost on HACS Segments. The models are trained for half of the full training cycle (15 epochs).

# head	0.5	0.75	0.95	Avg.	FLOPs/M
1	38.62	25.25	7.94	25.57	100.2
2	40.30	26.37	8.09	26.52	100.2
4	40.74	28.41	10.51	28.30	100.3
8	41.20	28.52	10.63	28.49	100.5
16	41.07	28.35	10.23	28.31	100.9

to 141 ms. With segment refinement enabled, the average time cost per video becomes 155 ms, which is still very efficient compared with state-of-the-art methods.

Effects of the numbers of encoder layers and decoder layers. We evaluate TadTR with different numbers of encoder layers (L_E) and decoder layers (L_D) and report results in Table 6. With L_D fixed, the best performance is achieved when L_E is 2. Larger L_E gives inferior results probably due to the difficulty of training. Therefore, we set L_E to 2. With L_E fixed, the average mAP increases by 2.03% when L_D increases from 2 to 4. Larger L_D gives a slightly lower performance. Therefore we suggest setting L_D to 4.

Effect of the number of sampling points. Table 7 compares the performance and computation cost using different numbers of sampling points K in TDA modules on HACS Segments. We observe that moderately increasing K improves the performance, as more temporal details can be captured. The best performance is achieved at $K = 4$. The number of sampling points has little impact on the computation cost.



Figure 6. actionness regression improves the ranking of detections. In each of the above cases, the more accurate obtains a lower score than the less accurate one before rescore. With the new scores (red color) applied, the ranking order turns satisfactory.

Effect of the number of attention heads. Table 8 compares the performance and computation cost using different number of attention heads M on HACS Segments. It is observed that that moderately increasing M boosts the performance, as more diverse features can be learned. The performance is saturated at $M = 8$. Similar to the number of sampling points, the number of attention heads has little impact on the computation cost.

Choices of the classification cost. For the classification cost in Equation 7, we explore two choices, focal loss (the default setting; non-linear) and negative probability (linear). The former results in an average mAP of 32.09%, superior to the latter (30.83%). We conjecture that the non-linear cost penalizes negative matching pairs harder and enlarges the difference in matching cost between negative pairs and positive pairs, which can stabilize instance matching and better suppress duplicate predictions. The former benefit is indicated by the faster convergence. The evidence of the latter benefit is that large N_q (e.g., 100) will cause duplicate predictions when the linear cost is used. Focal loss bypasses this issue. Therefore focal loss is a better choice.

4.4. Visualization

Visualization of action queries. Fig. 7 illustrates the distribution of locations and scales (lengths) of output actions associated with each action query. We observe that each query produces action predictions in certain locations and scales. For example, we observe that the first and the second queries are responsible for actions near the ending of a video and actions near the starting of a video, respectively. Different locations and scales are covered by a small number of queries. It means that the detector learns the distribution of actions in the training dataset. This is more flexible and efficient than the handcrafted anchor design in previous methods.

Visualization of attention. Fig. 8 visualizes attention of the last encoder layer and the last decoder layer. We use

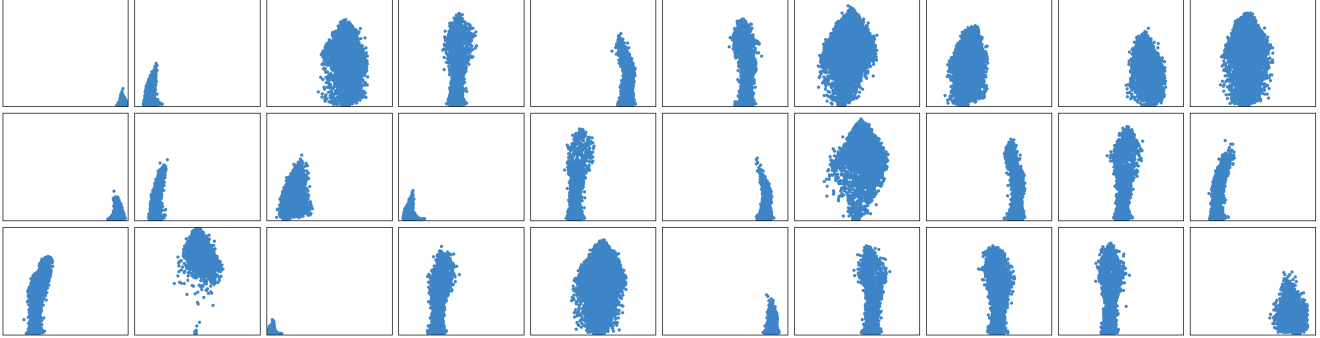


Figure 7. Distribution of all output actions on all videos from HACS Segments validation set for 30 query slots with action queries. In each 1-by-1 square, an action prediction predicted from the corresponding action query is represented as a point, and the horizontal and vertical coordinates are the coordinate of the center and the length normalized by the video length.

different colors to distinguish different attention heads. We observe that: (1) Different attention heads focus on different temporal regions and scales. The red and the pink points are sparsely distributed on the left side of a reference point. The blue and the purple points are sparsely distributed on the right. Other points are near the referent points. (2) Sampling points in the decoder almost cover the same temporal extent of an action prediction, providing a very large receptive field. Differently, sampling points in the encoder have a more flexible distribution, capturing a moderate amount of context.

5. Conclusion

We propose TadTR, a simple end-to-end method for temporal action detection (TAD) based on Transformer. It views the TAD task as a direct set prediction problem and maps a series of learnable embeddings to action instances in parallel by adaptively extracting temporal context in the video. It simplifies the pipeline of TAD and removes hand-crafted components such as anchor setting and post-processing. We make three improvements to enhance the Transformer with locality awareness to better adapt to the TAD task. Extensive experiments validate the remarkable performance and efficiency of TadTR and the effectiveness of different components. TadTR achieves state-of-the-art or competitive performance on HACS Segments, THU-MOS14, and ActivityNet-1.3 with lower computation costs. We hope that our work could trigger the development of vision Transformers and efficient models for temporal action detection.

In this work, TadTR is based on offline extracted features. Actually the video encoder can be jointly optimized with TadTR, which is investigated in our follow-up work [22]. In the future, we plan to explore temporal action detector purely based on Transformers.

References

- [1] Humam Alwassel, Silvio Giancola, and Bernard Ghanem. Tsp: Temporally-sensitive pretraining of video encoders for localization tasks. In *ICCV Workshops*, 2021.
- [2] Jimmy Lei Ba, Jamie Ryan Kiros, and Geoffrey E Hinton. Layer normalization. *arXiv preprint arXiv:1607.06450*, 2016.
- [3] Yueran Bai, Yingying Wang, Yunhai Tong, Yang Yang, Qiyue Liu, and Junhui Liu. Boundary content graph neural network for temporal action proposal generation. In *ECCV*, pages 121–137, 2020.
- [4] Gedas Bertasius, Heng Wang, and Lorenzo Torresani. Is space-time attention all you need for video understanding? In *ICML*, July 2021.
- [5] Shyamal Buch, Victor Escorcia, Chuanqi Shen, Bernard Ghanem, and Juan Carlos Niebles. Sst: Single-stream temporal action proposals. In *CVPR*, pages 6373–6382, 2017.
- [6] Fabian Caba Heilbron, Juan Carlos Niebles, and Bernard Ghanem. Fast temporal activity proposals for efficient detection of human actions in untrimmed videos. In *CVPR*, pages 1914–1923, 2016.
- [7] Fabian Caba Heilbron, Victor Escorcia, Bernard Ghanem, and Juan Carlos Niebles. Activitynet: A large-scale video benchmark for human activity understanding. In *CVPR*, pages 961–970, 2015.
- [8] Nicolas Carion, Francisco Massa, Gabriel Synnaeve, Nicolas Usunier, Alexander Kirillov, and Sergey Zagoruyko. End-to-end object detection with transformers. In *ECCV*, pages 213–229, 2020.
- [9] Joao Carreira and Andrew Zisserman. Quo vadis, action recognition? a new model and the kinetics dataset. In *CVPR*, pages 4724–4733, 2017.
- [10] Yu-Wei Chao, Sudheendra Vijayanarasimhan, Bryan Seybold, David A Ross, Jia Deng, and Rahul Sukthankar. Rethinking the faster r-cnn architecture for temporal action localization. In *CVPR*, pages 1130–1139, 2018.
- [11] Victor Escorcia, Fabian Caba Heilbron, Juan Carlos Niebles, and Bernard Ghanem. Daps: Deep action proposals for action understanding. In *ECCV*, pages 768–784, 2016.

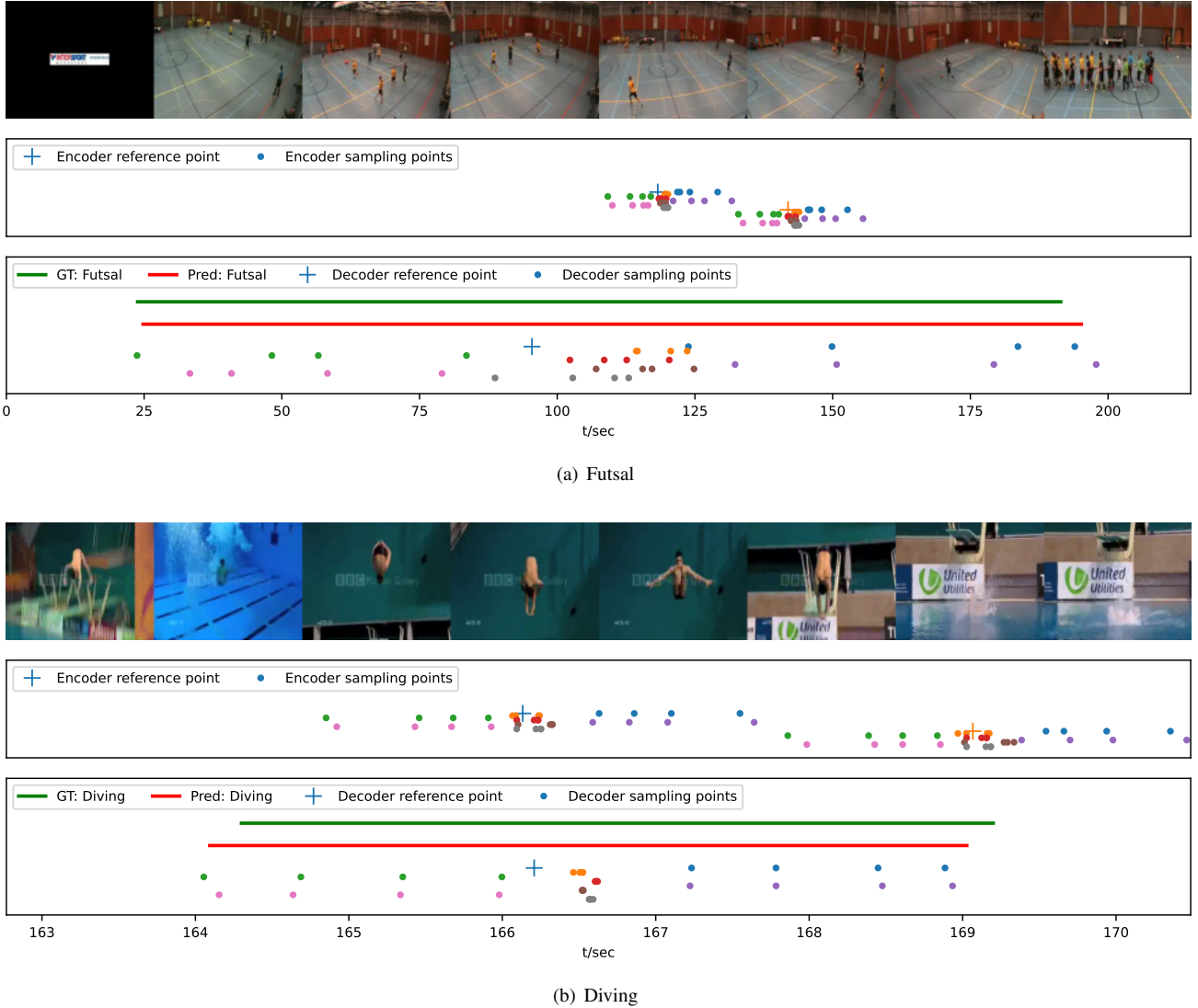


Figure 8. Visualization of attention. Each subfigure is composed of three rows. The first row is uniformly sampled video frames. The second row visualizes the attention at two randomly picked reference points in the last encoder layer. The third row visualizes the attention for the predicted action in the last decoder layer. Sampling points in different attention heads are in different colors. We separate the sampling points in different heads vertically for better readability. Best viewed in color.

- [12] Jiyang Gao, Kan Chen, and Ram Nevatia. Ctap: Complementary temporal action proposal generation. In *ECCV*, September 2018.
- [13] Jiyang Gao, Zhenheng Yang, Chen Sun, Kan Chen, and Ram Nevatia. Turn tap: Temporal unit regression network for temporal action proposals. In *ICCV*, pages 3648–3656, 2017.
- [14] Rohit Girdhar, Joao Carreira, Carl Doersch, and Andrew Zisserman. Video action transformer network. In *CVPR*, pages 244–253, 2019.
- [15] Kaiming He, Georgia Gkioxari, Piotr Dollár, and Ross Girshick. Mask r-cnn. In *ICCV*, pages 2961–2969, 2017.
- [16] YG Jiang, Jingen Liu, A Roshan Zamir, G Toderici, I Laptev, Mubarak Shah, and Rahul Sukthankar. Thumos challenge: Action recognition with a large number of classes, 2014.
- [17] Chuming Lin, Chengming Xu, Donghao Luo, Yabiao Wang, Ying Tai, Chengjie Wang, Jilin Li, Feiyue Huang, and Yanwei Fu. Learning salient boundary feature for anchor-free temporal action localization. In *CVPR*, pages 3320–3329, 2021.
- [18] Tianwei Lin, Xiao Liu, Xin Li, Errui Ding, and Shilei Wen. Bmn: Boundary-matching network for temporal action proposal generation. In *ICCV*, pages 3889–3898, 2019.
- [19] Tianwei Lin, Xu Zhao, and Zheng Shou. Single shot temporal action detection. In *ACM MM*, pages 988–996, 2017.
- [20] Tianwei Lin, Xu Zhao, Haisheng Su, Chongjing Wang, and Ming Yang. Bsn: Boundary sensitive network for temporal action proposal generation. In *ECCV*, September 2018.
- [21] Daochang Liu, Tingting Jiang, and Yizhou Wang. Complete-

ness modeling and context separation for weakly supervised temporal action localization. In *CVPR*, pages 1298–1307, 2019.

[22] Xiaolong Liu, Song Bai, and Xiang Bai. An empirical study of end-to-end temporal action detection. In *Proceedings of the IEEE/CVF Conference on Computer Vision and Pattern Recognition*, pages 20010–20019, 2022.

[23] Xiaolong Liu, Yao Hu, Song Bai, Fei Ding, Xiang Bai, and Philip H. S. Torr. Multi-shot temporal event localization: A benchmark. In *CVPR*, pages 12596–12606, June 2021.

[24] Yuan Liu, Lin Ma, Yifeng Zhang, Wei Liu, and Shih-Fu Chang. Multi-granularity generator for temporal action proposal. In *CVPR*, pages 3604–3613, 2019.

[25] Fuchen Long, Ting Yao, Zhaofan Qiu, Xinmei Tian, Jiebo Luo, and Tao Mei. Gaussian temporal awareness networks for action localization. In *CVPR*, pages 344–353, 2019.

[26] Ilya Loshchilov and Frank Hutter. Decoupled weight decay regularization. In *ICLR*, 2017.

[27] Fan Ma, Linchao Zhu, Yi Yang, Shengxin Zha, Gourab Kundu, Matt Feiszli, and Zheng Shou. Sf-net: Single-frame supervision for temporal action localization. In *ECCV*, pages 420–437. Springer, 2020.

[28] Shugao Ma, Leonid Sigal, and Stan Sclaroff. Learning activity progression in lstms for activity detection and early detection. In *CVPR*, June 2016.

[29] Megha Nawhal and Greg Mori. Activity graph transformer for temporal action localization. *arXiv preprint arXiv:2101.08540*, 2021.

[30] Phuc Nguyen, Ting Liu, Gautam Prasad, and Bohyung Han. Weakly supervised action localization by sparse temporal pooling network. In *CVPR*, pages 6752–6761, 2018.

[31] Sujoy Paul, Sourya Roy, and Amit K. Roy-Chowdhury. W-talc: Weakly-supervised temporal activity localization and classification. In *ECCV*, September 2018.

[32] Alexander Richard and Juergen Gall. Temporal action detection using a statistical language model. In *CVPR*, pages 3131–3140, 2016.

[33] Zheng Shou, Jonathan Chan, Alireza Zareian, Kazuyuki Miyazawa, and Shih-Fu Chang. Cdc: Convolutional-deconvolutional networks for precise temporal action localization in untrimmed videos. In *ICCV*, pages 1417–1426, 2017.

[34] Zheng Shou, Hang Gao, Lei Zhang, Kazuyuki Miyazawa, and Shih-Fu Chang. Autoloc: Weakly-supervised temporal action localization in untrimmed videos. In *ECCV*, pages 154–171, 2018.

[35] Zheng Shou, Dongang Wang, and Shih-Fu Chang. Temporal action localization in untrimmed videos via multi-stage cnns. In *CVPR*, pages 1049–1058, 2016.

[36] Rui Su, Dong Xu, Lu Sheng, and Wanli Ouyang. Pcg-tal: Progressive cross-granularity cooperation for temporal action localization. *IEEE Transactions on Image Processing*, 30:2103–2113, 2021.

[37] Chen Sun, Austin Myers, Carl Vondrick, Kevin Murphy, and Cordelia Schmid. Videobert: A joint model for video and language representation learning. In *ICCV*, pages 7464–7473, 2019.

[38] Jing Tan, Jiaqi Tang, Limin Wang, and Gangshan Wu. Relaxed transformer decoders for direct action proposal generation. In *ICCV*, pages 13526–13535, October 2021.

[39] Ashish Vaswani, Noam Shazeer, Niki Parmar, Jakob Uszkoreit, Llion Jones, Aidan N. Gomez, Łukasz Kaiser, and Illia Polosukhin. Attention is all you need. In *NIPS*, pages 5998–6008, 2017.

[40] Limin Wang, Yuanjun Xiong, Dahua Lin, and Luc Van Gool. Untrimmednets for weakly supervised action recognition and detection. In *CVPR*, pages 4325–4334, 2017.

[41] Limin Wang, Yuanjun Xiong, Zhe Wang, Yu Qiao, Dahua Lin, Xiaoou Tang, and Luc Van Gool. Temporal segment networks: Towards good practices for deep action recognition. In *ECCV*, pages 20–36, 2016.

[42] Huijuan Xu, Abir Das, and Kate Saenko. R-c3d: region convolutional 3d network for temporal activity detection. In *ICCV*, pages 5794–5803, 2017.

[43] Mengmeng Xu, Chen Zhao, David S Rojas, Ali Thabet, and Bernard Ghanem. G-TAD: Sub-graph localization for temporal action detection. In *CVPR*, pages 10156–10165, 2020.

[44] Le Yang, Houwen Peng, Dingwen Zhang, Jianlong Fu, and Junwei Han. Revisiting anchor mechanisms for temporal action localization. *IEEE Transactions on Image Processing*, 29:8535–8548, 2020.

[45] Serena Yeung, Olga Russakovsky, Greg Mori, and Li Fei-Fei. End-to-end learning of action detection from frame glimpses in videos. In *CVPR*, pages 2678–2687, 2016.

[46] Tan Yu, Zhou Ren, Yuncheng Li, Enxu Yan, Ning Xu, and Junsong Yuan. Temporal structure mining for weakly supervised action detection. In *ICCV*, pages 5522–5531, 2019.

[47] Jun Yuan, Bingbing Ni, Xiaokang Yang, and Ashraf A Kasim. Temporal action localization with pyramid of score distribution features. In *CVPR*, pages 3093–3102, 2016.

[48] Ze-Huan Yuan, Jonathan C Stroud, Tong Lu, and Jia Deng. Temporal action localization by structured maximal sums. In *CVPR*, volume 2, page 7, 2017.

[49] Runhao Zeng, Wenbing Huang, Mingkui Tan, Yu Rong, Peilin Zhao, Junzhou Huang, and Chuang Gan. Graph convolutional networks for temporal action localization. In *ICCV*, pages 7094–7103, 2019.

[50] Hang Zhao, Antonio Torralba, Lorenzo Torresani, and Zhicheng Yan. HACS: human action clips and segments dataset for recognition and temporal localization. In *ICCV*, pages 8667–8677, 2019.

[51] Peisen Zhao, Lingxi Xie, Chen Ju, Ya Zhang, Yanfeng Wang, and Qi Tian. Bottom-up temporal action localization with mutual regularization. In *ECCV*, 2020.

[52] Yue Zhao, Yuanjun Xiong, Limin Wang, Zhirong Wu, Xiaoou Tang, and Dahua Lin. Temporal action detection with structured segment networks. *ICCV*, pages 2914–2923, 2017.

[53] Yue Zhao, Bowen Zhang, Zhirong Wu, Shuo Yang, Lei Zhou, Sijie Yan, Limin Wang, Yuanjun Xiong, Wang Yali, Dahua Lin, Yu Qiao, and Xiaoou Tang. CUHK & ETHZ & SIAT submission to ActivityNet challenge 2017. *arXiv preprint arXiv:1710.08011*, pages 20–24, 2017.

- [54] Luowei Zhou, Yingbo Zhou, Jason J Corso, Richard Socher, and Caiming Xiong. End-to-end dense video captioning with masked transformer. In *CVPR*, pages 8739–8748, 2018.
- [55] Linchao Zhu and Yi Yang. Actbert: Learning global-local video-text representations. In *CVPR*, pages 8746–8755, 2020.
- [56] Xizhou Zhu, Weijie Su, Lewei Lu, Bin Li, Xiaogang Wang, and Jifeng Dai. Deformable detr: Deformable transformers for end-to-end object detection. In *ICLR*, 2021.